Journal Pre-proof


Revealing design archetypes and flexibility in e-molecule import pathways using Modeling to Generate Alternatives and interpretable machine learning

Mahdi Kchaou, Francesco Contino, Diederik Coppitters

PII: S3117-5872(26)00003-0
DOI: https://doi.org/10.1016/j.ptx.2026.100003
Reference: PTX 100003

To appear in: *Power-to-X*

Received date: 25 March 2026
Revised date: 30 June 2026
Accepted date: 20 August 2026

Please cite this article as: Mahdi Kchaou, Francesco Contino, Diederik Coppitters, Revealing design archetypes and flexibility in e-molecule import pathways using Modeling to Generate Alternatives and interpretable machine learning, *Power-to-X* (2026), doi: https://doi.org/10.1016/j.ptx.2026.100003

**Highlights**

- Structural uncertainties are investigated for hydrogen import projects.
- Modeling to Generate Alternatives is coupled with clustering and decision trees to extract interpretable insights.
- MGA brings great design flexibility within a 10
- Wind, solar, and storage are not strictly required to achieve near-optimal costs.
- Carrier choice ($NH_3$, $CH_4$, MeOH) depends on renewable deployment and storage constraints.

# Revealing design archetypes and flexibility in e-molecule import pathways using Modeling to Generate Alternatives and interpretable machine learning

Mahdi Kchaou[a,*], Francesco Contino[a], Diederik Coppitters[a]

[a]*Institute of Mechanics, Materials and Civil Engineering (iMMC), Université catholique de Louvain (UCLouvain), Place du Levant, 2, 1348 Louvain-la-Neuve, Belgium*

**Abstract**

Given the central role of green e-molecule imports in the European energy transition, many studies optimize import pathways and identify a single cost-optimal solution. However, cost-optimal designs may be sensitive to real-world constraints, as regulatory, spatial, and stakeholder considerations are often difficult to represent in optimization models and may affect their practical feasibility. To address this limitation, we use a greenfield, snapshot capacity expansion model of a hydrogen production and transport supply chain from Morocco to Belgium, considering hydrogen, ammonia, methane, and methanol as import carriers under a fixed hydrogen demand. Using the Modeling All Alternatives (MAA) method, which is a Modeling to Generate Alternatives (MGA) approach, we generate a large and diverse set of near-optimal solutions within an acceptable cost margin, enabling the exploration of design flexibility under structural uncertainties. Given the complexity of interpreting a large number of near-optimal alternatives, interpretable machine learning is applied to extract actionable insights from the large solution space. Results show that hydrogen transported via pipelines is the lowest-cost option (91 €/MWh), while methane transported via pipelines is the most expensive (213 €/MWh). Moreover, MGA reveals a broad near-optimal space with great flexibility: solar, wind, and storage are not strictly required to remain within 10% of the cost optimum. Wind capacity can reach up to 20 GW, PV capacity up to 40 GW, battery capacity up to 60 GWh, and hydrogen storage up to 162 GWh, depending on the carrier. Limited access to wind energy favors systems with higher electrolyzer and solar capacities combined with storage, particularly in methanol pathways. On the other hand, limited storage availability favors wind-dominated systems, with ammonia or methane pathways becoming more attractive. These results demonstrate that multiple structurally distinct supply chains are economically viable, giving stakeholders broad room for decision-making.

*Keywords:* E-molecules, Hydrogen, Interpretable Machine Learning, Modeling to Generate Alternatives, Decision Trees, Energy System Optimization Model

*Corresponding author
*Email address:* `mahdi.kchaou@uclouvain.be` (Mahdi Kchaou)

## 1. Introduction

The EU aims to import 10 million tonnes of hydrogen by 2030 to meet its carbon-reduction target [1]. The general vision is that hydrogen will be produced in remote, renewable-rich regions using electrolysis powered by wind or solar [2]. Because transporting pure hydrogen over long distances remains technically challenging, several studies have investigated hydrogen-derived carriers such as ammonia. Verleysen et al. [3] assessed the production of renewable ammonia in Morocco and its export to Belgium for direct ammonia use. In contrast, Roos et al. [4] evaluated ammonia production in South Africa followed by export to Europe and Japan, where the ammonia is reconverted into hydrogen at the destination. Once imported by the densely populated, industrialized area, hydrogen has the potential to serve multiple roles, from long-distance energy transport and seasonal storage to the decarbonization of heavy industry such as steel, chemicals, and cement [5].

Several studies have examined the techno-economic aspects of producing and transporting hydrogen-based energy carriers [6]. The Hydrogen Import Coalition [7], for example, assessed imports of renewable energy via hydrogen carriers shipped from various locations to Belgium, demonstrating both technical feasibility and cost-effectiveness. At a small scale (transport distances of 250 km), Dias et al. [8] showed that among four carriers: hydrogen, ammonia, methane, and methanol, hydrogen is the least favorable option for a production, transport and reconversion to electricity chain. In contrast, the other carriers are more cost-competitive, with methanol emerging as the cheapest option. This is largely due to their easier handling and the availability of existing infrastructure, as is the case for methane. At a larger scale, Hampp et al. [9] evaluated imports of e-chemicals from diverse regions to Germany. They found that all e-chemicals could be imported at lower cost than producing them domestically. However, when meeting hydrogen demand directly, importing hydrogen was more attractive than importing carriers and converting them upon arrival. Other comparative studies suggest that ammonia is the most economical at large scales, while methanol can be competitive at small scales if low-cost $CO_2$ is available [10]. Johnston et al. [11] further showed that transporting ammonia by ship is the cheapest option for both Tokyo and Rotterdam. Yet results are not uniform: Galimova et al. [12] report that renewable hydrogen imports from North Africa and South America may be more expensive than domestic hydrogen production in Germany and Finland. Their other analysis [13] further shows that ammonia imports from the same exporting regions can be economically attractive for both countries. Overall, these findings underscore that conclusions depend strongly on techno-economic assumptions and case-specific conditions.

A common limitation of these studies is that they rely on deterministic parameters [14]. In reality, both technical and economic inputs are subject to uncertainties: e.g. solar irradiance ($\pm 3.11\%$ in Morocco [3]), technology efficiencies (from 0.532 to 0.648 kWh/$kg_{NH_3}$ for the Haber–Bosch unit [3]), and investment costs (from 455 to 5317€ /kW for the Haber–Bosch unit [3]). Such uncertainties can affect system performance [15].

To account for this, many studies conduct sensitivity tests, varying one assumption at a time [9]. While useful, this approach cannot fully capture how uncertainties propagate through models and simultaneously impact the performance of the system, including synergistic and antagonistic interactions. For this purpose, systematic Uncertainty Quantification (UQ) is required. To assess the importance of parametric uncertainty, Coppitters et al. [16] used the polynomial chaos expansion method to quantify uncertainties in a coupled PV-electrolyzer system. They reported a robust Levelized Cost of Hydrogen (LCOH) of 6.4 €/kg in Johannesburg, with a standard deviation of 0.74 €/kg, while the discount rate was identified as the main driver of cost variation. In a similar hydrogen production context, Wolf et al. [17] applied uncertainty quantification to estimate the 2050 LCOH in Northern Africa and Europe, and found large uncertainty ranges: PV-based hydrogen in Spain varied from about 1.66 €/kg to 3.12 €/kg, and in Morocco and Algeria from about 1.70–1.80 €/kg up to 3.2–3.3 €/kg.

In addition to parametric uncertainties, structural uncertainties linked to decision-making play a critical role [18]. Unlike parameter uncertainty, which assumes the model itself is correct, real projects also face uncertainty about goals, system boundaries, and stakeholder preferences. These hard to quantify uncertainties can, in practice, fundamentally alter what is considered optimal in theory. Examples from past renewable projects illustrate these effects. Social resistance has delayed or canceled developments, such as the Nevada PV farm opposed by local communities [19]. Technological limits for large-scale batteries, like rate capability, lifespan, and raw material needs, continue to hinder their deployment despite favorable techno-economic projections [20]. Policy shifts, such as Morocco's move from Concentrated Solar Power to PV coupled with storage [21], can redirect investment away from designs once seen as optimal. Legal disputes, as with wind projects in Spain [22], further illustrate how institutional processes can reshape or halt projects.

For hydrogen import pathways, these uncertainties are especially important. Choices about carriers, the balance between imports and domestic production, or the expansion of ports and pipelines depend not only on costs but also on politics, lobbying, regulation, and public acceptance. Geopolitical analyses show that international relations and energy security concerns can determine which routes are viable, even when cheaper options exist [23]. In Europe, lobbying by industry groups has been shown to influence hydrogen policy and favor certain pathways [24]. Public acceptance also matters: survey evidence [25] shows that awareness, trust, and local concerns can delay or block hydrogen projects. Thus, what appears optimal in techno-economic models may prove politically unworkable, socially resisted, or institutionally blocked.

A way to address non-quantifiable or structural uncertainties in energy system modeling is Modeling to Generate Alternatives (MGA). Rather than searching only for the lowest-cost solution, MGA identifies near-optimal configurations that differ in design, thereby allowing qualitative, institutional, or acceptance criteria to be considered when selecting among them [26]. The approach was first formalized in the context of water resources planning through the Hop-Skip-Jump method [27], and was later adapted to energy systems by DeCarolis [28], who demonstrated how structurally diverse yet cost-competitive energy futures can reveal trade-offs hidden in single-optimum analyses. Recent developments have extended MGA methods to improve the exploration of near-optimal solution spaces. Neumann et al. [29] proposed a min/max formulation to explore the range of decision variables under predefined cost slack, while Lombardi et al. [30] generated spatially distinct energy system configurations to assess alternative regional deployment strategies. Pedersen et al. [31] further advanced the methodology by characterizing the full near-optimal solution space through its enclosing convex hull. Although MGA has been applied extensively in large-scale energy system studies, particularly in Europe, its application to local-scale systems such as hydrogen production and transport networks remains limited. For instance, Sinha et al. [32] showed that hydrogen deployment diverges significantly across near-optimal decarbonization pathways for the U.S. energy system, ranging from electrolytic hydrogen to fossil-based hydrogen with carbon capture, with substantial variation in sectoral uptake. Despite these advances, MGA studies often generate a large number of near-optimal solutions that can be difficult to interpret, particularly from a decision-making perspective. To address this challenge, recent studies have employed clustering techniques to identify representative system configurations from large sets of alternatives. For example, Prina et al. [33] used clustering methods to distill large collections of near-optimal solutions into a smaller set of representative configurations. Baader et al. [34] further combined clustering with decision trees to derive interpretable decision rules and streamline the analysis of energy transition scenarios. While these methodological developments have improved the handling of structural uncertainty, most techno-economic assessments of hydrogen import pathways remain focused on deterministic cost optimization under techno-centric assumptions. Structural uncertainties arising from decision-making processes, institutional constraints, and stakeholder preferences have received little attention, even though they can strongly influence the practical feasibility of hydrogen projects. As a result, existing analyses provide limited guidance on how alternative preferences and constraints may shape hydrogen production and transport pathways.

To address this gap, we investigate how non-quantifiable factors influence the design of hydrogen import pathways. Specifically, we examine preferences related to the deployment of key technologies, including photovoltaic installations, wind turbines, batteries, electrolyzers, and hydrogen storage, as well as the selection of hydrogen carriers (hydrogen, methane, methanol, and ammonia). To capture flexibility in decision-making, we apply the Modeling All Alternatives (MAA) approach [31], which is an MGA method. The MAA method defines the entire near-optimal space by constructing its enclosing convex hull, allowing for the exploration of a diverse set of near-optimal solutions within a reasonable cost slack. This approach is applied to an energy system optimization model for hydrogen production and transportation developed using PyPSA. Because the resulting near-optimal solution space can be vast and difficult to interpret, we complement MAA with interpretable machine learning techniques. Specifically, clustering is used to identify representative design archetypes, while decision trees are employed to derive transparent decision rules and quantify the consequences of key design choices. Together, these methods transform a large ensemble of near-optimal solutions into actionable insights for decision-makers.

Overall, this study provides practical guidance for decision-makers facing location-specific, institutional, or stakeholder-driven constraints affecting the deployment of renewable generation, storage technologies, and hydrogen carrier options.

In this paper, we first present the hydrogen import optimization model, the MGA approach, and the interpretable machine learning methods (Section 2). The results (Section 3) begin with a description of the optimized solutions for the different pathways (carriers and transportation methods), along with a cost breakdown to highlight the main cost drivers for each. Next, we present the near-optimal space, demonstrating the wide variety of designs that remain within a near-optimal cost range for each pathway. Finally, we present the results from the interpretable machine learning analysis, offering key insights into the impact of decisions, such as the absence of certain technologies, on the final design configuration. We also identify clusters of solutions that point to a limited set of design archetypes that can be pursued. Section 4 provides a discussion of the results and the main limitations of the study. Section 5 concludes this paper with the main takeaways.

## 2. Methods

The methods section begins by outlining the energy system optimization model used for the techno-economic optimization of the production and transportation pathways for each carrier: hydrogen, methane, methanol, and ammonia (Subsection 2.1). Subsection 2.2 then introduces the case study implemented in the model, focusing on a renewable-rich production site in Morocco and a high-demand, densely populated import location in Belgium. Next, Subsection 2.3 presents the MGA approach, which generates diverse near-optimal solutions for the different pathways. This provides a set of maximally distinct alternatives within an acceptable cost range for producing and transporting hydrogen and other carriers, addressing non-quantifiable uncertainties in decision-making. Finally, Subsection 2.4 details the interpretable machine learning method used to translate the numerous near-optimal alternatives into clear design guidelines.

### *2.1. Energy system optimization model for hydrogen production and transportation*

The hydrogen supply chain in this study is modeled using the TRACE model [9], a linear programming framework developed within PyPSA [35] to evaluate international supply chains for hydrogen and other electrofuels. TRACE represents a single export–import corridor between a production site and a demand location and follows a greenfield, snapshot capacity expansion approach. The model optimizes investments and operation to satisfy a fixed hydrogen demand while minimizing total system costs. As such, it does not consider $CO_2$ reduction targets, competition among multiple exporting regions, or interactions with other energy systems. The model determines the cost-optimal deployment and operation of renewable generation, conversion, storage, and transport infrastructure. Solar and wind generation are represented at hourly resolution. The system includes desalination, direct air capture (DAC), and air separation units (ASU) to supply water, carbon dioxide, and nitrogen for fuel synthesis. Buffer storage is modeled to satisfy must-run constraints in chemical synthesis plants, and losses are considered in processes such as liquefaction, compression, and boil-off. The supply chain ends at the import terminal: downstream distribution, end-use and the use of by-products are not represented.

The objective function minimizes the total annualized system cost, which includes:

- Capital expenditures for generation, conversion, storage, and transport technologies ($C_{\mathrm{i}}$), annualized using an annuity factor based on the weighted average cost of capital (WACC) and the technical lifetime:
$$A_i = \frac{(1+r)^{n_{\mathrm{i}}} \cdot r}{(1+r)^{n_{\mathrm{i}}} - 1},$$
where $r$ is the interest rate, i denotes the component index and $n_{\mathrm{i}}$ its lifetime.
- Fixed operation and maintenance (O&M) costs ($O_{\mathrm{i}}$).

The annualized cost for each component is therefore:

$$c_{\mathrm{i}} = C_{\mathrm{i}} \cdot A_{\mathrm{i}} + O_{\mathrm{i}},$$

and the optimization problem is formulated as:

$$\underset{x_{\mathrm{i}}}{\text{minimize}} \sum_{\mathrm{i}} c_{\mathrm{i}} \cdot x_{\mathrm{i}}.$$

where $x_{\mathrm{i}}$ denotes the capacity of each component to be optimized.

The supply chain is structured as follows. Renewable electricity is generated from solar and wind sources (PV panels and wind turbines), while storage technologies (batteries and hydrogen storage) are included to mitigate intermittency, as the system is modeled as an islanded configuration with no connection to the power grid. Additional storage tanks for liquid carriers are considered at both the export and import ports to act as buffers around the shipping process. Because liquid carrier storage is significantly cheaper than hydrogen storage, the model can capture the potential trade-off between the lower storage costs of hydrogen-derived carrier systems and the additional costs and efficiency losses associated with synthesis and reconversion. Hydrogen is produced through PEM electrolysis, coupled with a desalination unit that supplies pure water from seawater. From this point, our analysis considers four possible hydrogen carriers: hydrogen, methane, ammonia, and methanol, and two transportation options: pipeline and shipping. Hydrogen can either be transported directly in gaseous form by pipeline or liquefied and shipped, with boil-off losses accounted for during shipping. Methane is produced via catalytic methanation of hydrogen with carbon dioxide captured from the air using DAC, and is either transported by pipeline in gaseous form or liquefied for shipping. Ammonia is synthesized through the Haber–Bosch process, combining hydrogen with nitrogen from an ASU, transported as liquid either by pipeline or ship. Methanol is produced from hydrogen and carbon dioxide through catalytic synthesis and can likewise be transported by pipeline or ship. At the import terminal, all carriers are converted back to gaseous hydrogen to provide a uniform end product: liquid hydrogen is evaporated, ammonia is cracked, and methane and methanol are reformed. The potential use of by-products from these conversion processes is not accounted for in the model. All techno-economic parameters, including process efficiencies, energy demands, and cost assumptions, follow the values reported in Hampp et al. [9]. A schematic overview of the modeled supply chain is shown in Figure 1.

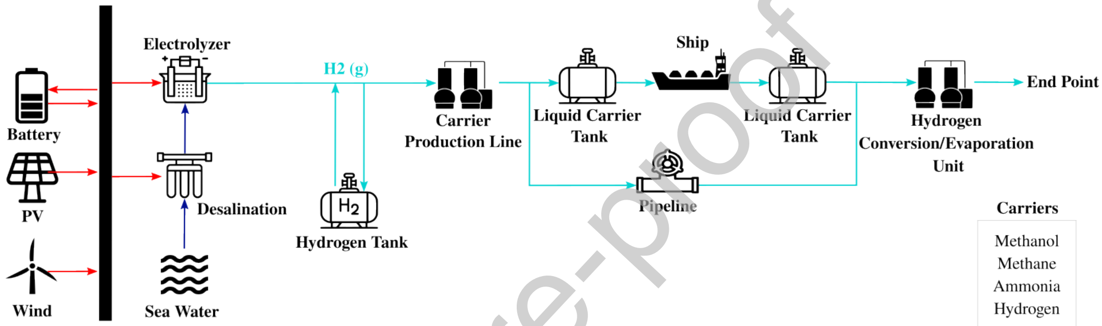


Figure 1: Overview of the hydrogen import supply chain. Renewable electricity from solar PV and wind turbines is used to produce hydrogen via PEM electrolysis, with seawater desalination providing the required feedwater. Battery storage balances the short-term variability of renewable generation, while hydrogen storage buffers supply before conversion. The produced hydrogen can then enter one of four carrier-specific synthesis pathways: (i) compression or liquefaction for direct hydrogen transport, (ii) catalytic methanation with captured $CO_2$ to produce synthetic methane, (iii) combination with nitrogen from an air separation unit in a Haber-Bosch process to produce ammonia, or (iv) catalytic synthesis with $CO_2$ to produce methanol. The resulting carriers are transported either by ship or pipeline to the import terminal, with liquid carriers requiring additional storage before and after shipping. At the import side, carriers go through reconversion: regasification for liquid hydrogen, reforming for methane and methanol, and cracking for ammonia, so that all pathways ultimately deliver gaseous hydrogen as a uniform end product.

### *2.2. Case study*

The case study considers an export-import corridor between Morocco and Belgium. Morocco is selected as the production site due to its abundant solar and wind resources, its established role as a front-runner in renewable energy deployment, and its strategic geographic position at the interface between Africa and Europe [36]. The renewable potential of Morocco is illustrated in Figure 2. The average capacity factor is 44% for wind and 29% for solar. While the monthly average solar energy remains consistent throughout the year, the monthly average wind energy exhibits seasonal variability, with higher output during the spring months.

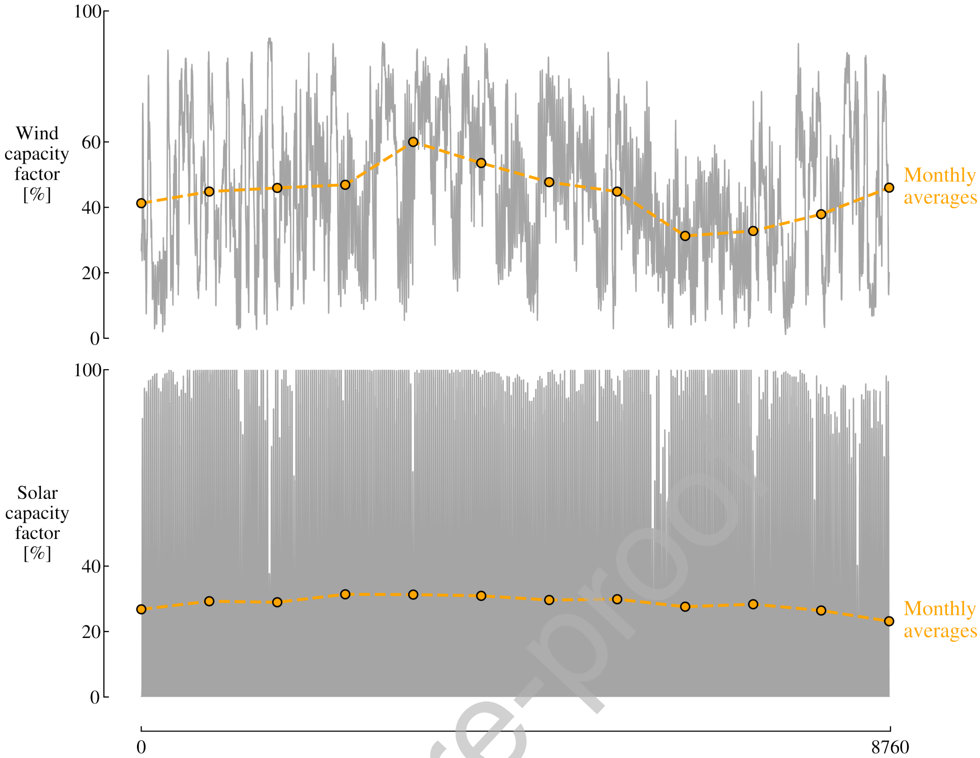


Figure 2: Renewable potential of Morocco, showing high wind and solar resources with average capacity factors of 44% and 29%, respectively. The monthly average of solar energy remains stable year-round, whereas wind energy is more variable, with the highest average potential during spring.

Belgium is chosen as the import destination, with an annual hydrogen import target of 20 $TWh_{H_2}$ (0.6 $Mt_{H_2}$), consistent with the ambition set in the Belgian federal hydrogen strategy [37]. The corridor represents a mid-distance trade route of 2517 km.

Overall, this study evaluates eight hydrogen import pathways, defined as unique combinations of four carriers (hydrogen, ammonia, methane, and methanol) and two transport modes (shipping and pipeline) along the Morocco–Belgium corridor. Each pathway is optimized independently, resulting in eight distinct optimal designs.

*2.3. Modeling to Generate Alternatives*

Energy system optimization models typically return a single least-cost solution. While this benchmark is useful, it is unlikely to be realized in practice. Technology costs are uncertain, performance differs across contexts, and political or social preferences may shift designs away from the mathematical optimum. It is therefore more informative to examine not only the strict cost-optimal configuration but also the broader set of near-optimal designs: solutions that are only slightly more expensive but structurally different. This helps identify which technologies are required across all cost-competitive designs and which are flexible, allowing trade-offs without large cost penalties.

The Modeling to Generate Alternatives (MGA) approach provides a structured way to achieve this. Following Pedersen et al. [31], we adopt the Modeling to Generate All Alternatives (MAA) method, which systematically maps the near-optimal solution space. Formally, let $f(x)$ denote the objective function and $x^*$ the optimal solution. The near-optimal space $W$ is defined as:

$$W = \{\, x \in X \mid f(x) \leq f(x^*)(1+\varepsilon) \,\}, \tag{1}$$

where $X$ is the feasible solution space and $\varepsilon$ is the slack parameter. This ensures that only solutions within a specified tolerance of the optimum are explored. In this study, $f(x)$ corresponds to the total annualized system cost, and $\varepsilon$ is set to 10% for each pathway individually, meaning that all solutions within 10% of the least-cost design of that pathway are considered near-optimal.

The algorithm then proceeds in two phases. The first phase defines the boundaries of the near-optimal space by constructing the convex hull [38], which is the smallest convex polyhedron enclosing all near-optimal solutions. To generate the points that define this convex hull, the objective function is modified from minimizing the total system cost to minimizing a weighted sum of the MGA variables of interest: PV, wind, electrolyzer, battery, and hydrogen storage tank capacities, while enforcing the MGA cost constraint:

$$\begin{aligned} \underset{x_{\mathrm{i}},\, \mathrm{i}\in V_{\mathrm{MGA}}}{\text{minimize}} \quad & \sum_{\mathrm{i}} w_{\mathrm{i}} \cdot x_{\mathrm{i}} \\ \text{s.t.} \quad & f(x) \leq f(x^*)(1+\varepsilon). \end{aligned} \tag{2}$$

The process begins by maximizing and minimizing each of the MGA variables and constructing a convex hull around the resulting solutions using the Quickhull algorithm. At each iteration, a set of $m$ weight vectors $\{w_k\}_{1\leq k\leq m}$ is generated such that they are normal to the faces of the convex hull obtained in the previous iteration. Using these weights, new points are explored, and a new convex hull is then constructed that encompasses both previously identified and newly identified solutions. This procedure is repeated, and the convex hull is iteratively updated until its volume converges.

Once the boundaries are mapped, the second phase samples solutions from the interior of the polyhedron. Because the whole problem is convex, any point inside the convex hull is also feasible and near-optimal. The polyhedron is divided into simpleces using the Qhull software [38], and random samples are drawn within these simplexes by computing a weighted sum of the vertices defining each simplex. Pedersen et al. [31] used the Bayesian bootstrap method to generate the weights, ensuring an even spread of points across the region. The outcome is a large set of alternative system designs that are distinct in structure, but all remain cost-competitive.

This method avoids the limitations of other MGA approaches, which often produce only a handful of alternatives without systematically exploring the entire near-optimal space, thereby risking the omission of important solutions. In contrast, the MAA method provides a comprehensive coverage of the near-optimal region while efficiently generating a large number of alternative solutions within seconds.

The MGA procedure is applied separately to each of the eight pathways described in Subsection 2.2, generating a diverse set of near-optimal designs for each pathway. This enables us to explore design trade-offs, such as between wind and PV, and to identify which technology choices are interdependent.

### *2.4. Interpretable machine learning*

The MGA approach (Subsection 2.3) generates a large set (in the order of $10^6$ with MAA) of near-optimal solutions with only a slight increase in cost. While this set provides a broad view of feasible and acceptable designs, the large number of solutions can make interpreting decisions and extracting meaningful insights a challenging task for decision-makers. To address this, we adopt the interpretable machine learning framework of [34], which translates a high-dimensional solution set into a small number of clear and interpretable decision rules.

The method begins by applying clustering algorithms to group the solutions. Each solution is assigned a cluster label, forming sets of configurations with similar characteristics. In our analysis, the decision variables consist of categorical variables, which are the binary indicators specifying the chosen transport carrier, and continuous variables representing the installed capacities of PV, wind turbines, electrolyzers, batteries, and hydrogen storage. When only continuous variables are involved, we use the $k$-means algorithm, whereas when both binary and continuous variables are present, we use $k$-prototypes clustering [39]. This method extends $k$-means by combining squared Euclidean distances for continuous variables with a simple matching dissimilarity for categorical variables. The overall dissimilarity between design $x_i$ and cluster centroid $c_j$ is defined as:

$$d(x_i, c_j) = \sum_{l \in \mathcal{C}} \big(x_{il} - c_{jl}\big)^2 \ + \ \gamma \sum_{m \in \mathcal{D}} \delta(x_{im}, c_{jm}), \tag{3}$$

where $x_i$ is the normalized vector of decision variables for design $i$, and $c_j$ is the centroid of cluster $j$. The index sets $\mathcal{C}$ and $\mathcal{D}$ refer to continuous and categorical variables, respectively. For a continuous variable $l \in \mathcal{C}$, the squared difference $(x_{il} - c_{jl})^2$ measures the distance in that dimension. For a categorical variable $m \in \mathcal{D}$, the function $\delta(x_{im}, c_{jm})$ equals zero if design $i$ and centroid $j$ share the same category, and one otherwise. The parameter $\gamma > 0$ controls the relative weight of categorical mismatches compared to continuous differences, ensuring that both binary carrier choices and continuous capacity decisions contribute to the clustering outcome. Low $\gamma$ values give more influence to continuous variables, whereas high values make categorical features dominant. In our case, $\gamma$ was set to 0.02. The automatic value obtained using the method proposed in [40] is $\gamma = 0.07$. After testing additional $\gamma$ values around the automatically calculated value, we selected $\gamma = 0.02$ because it produced clusters that performed better according to two evaluation metrics: the silhouette score [41] and the decision tree accuracy which is defined as:

$$\text{Accuracy} = \frac{1}{N}\sum_{i=1}^{N} \mathbf{1}(\hat{y}_i = y_i)\,, \tag{4}$$

where $N$ is the total number of samples, $y_i$ is the true cluster label of sample $i$, $\hat{y}_i$ is the cluster label predicted by the decision tree. A more detailed analysis is provided in the Supplementary Information.

In the second step, a decision tree (Classification and Regression Tree - CART) is trained [42], with the MGA decision variables as features and the cluster labels as targets. The decision tree identifies splits in the feature space by defining thresholds on feature values, ultimately mapping designs to their respective clusters. This yields a compact set of hierarchical rules that explain how different clusters arise. In this step, feature importances are calculated to identify which MGA decision variables have the greatest influence on the decision space. Feature importance is computed as the normalized total reduction in node impurity contributed by each feature across all splits of the decision tree.

The final step involves reassigning designs based on the decision tree's predictions. While most designs remain in their original clusters, those classified differently by the decision tree are reassigned accordingly. After this step, the clusters are defined by the splits and thresholds determined by the decision tree, providing a more interpretable and structured representation of the near-optimal space.

The selection of the number of clusters and the depth of the decision tree is based on a balance between accuracy and interpretability, and is detailed in the Supplementary Information.

We first apply this procedure using $k$-prototypes clustering on the full set of solutions generated by the MGA approach across the three hydrogen-derived shipping pathways (corresponding to ammonia, methane and methanol). This allows the clustering to capture both the design characteristics of each solution and the associated carrier choice. Similar patterns were observed for the pipeline case, therefore, we present only the shipping results here. The pipeline results can be found in the Supplementary Information. To further examine the structure of the near-optimal space, we then apply $k$-means clustering separately to each individual pathway. This second step captures within-pathway trade-offs, such as different balances between renewable generation and storage. Taken together, these two stages provide both a cross-pathway view of the solution space and a detailed understanding of the trade-offs within each pathway.



## 3. Results

In this section, we first discuss the cost-optimal configuration for each import pathway, followed by a detailed cost breakdown (Subsection 3.1). We then showcase the near-optimal solution space (Subsection 3.2), and finally streamline the large set of designs identified through this exploration using interpretable machine learning (Subsection 3.3).

### 3.1. Cost-optimal hydrogen import pathways

As a first step, we generate the cost-optimal solutions for each hydrogen import pathway. Hydrogen carrier pathways exhibit the lowest LCOH, while hydrogen-derived carriers: ammonia, methane, and methanol, show roughly twice the cost (Figure 3). In particular, hydrogen transported through pipelines achieves the

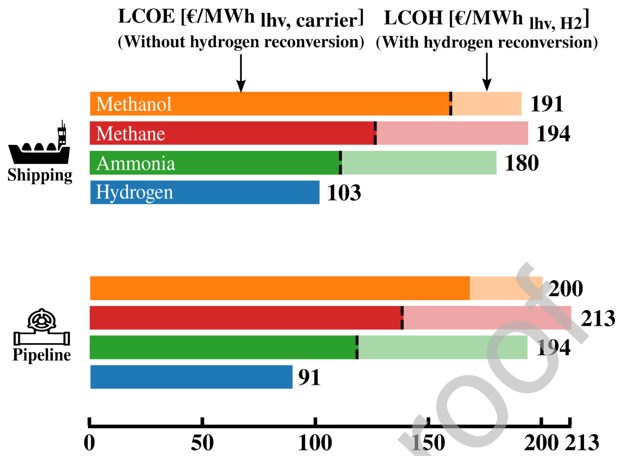


Figure 3: Hydrogen pathways (shipping and pipelines) are associated with the lowest LCOH, while hydrogen-derived carrier pathways exhibit nearly twice the cost. Among hydrogen-derived options, ammonia has the lowest LCOH, while methane has the highest. Excluding the reconversion step for hydrogen-derived carriers significantly reduces the LCOE difference, bringing them closer to hydrogen and making methane cheaper than methanol. This contrasts with the case including the conversion step, where methanol performs better as a hydrogen carrier, whereas methane appears more suitable as a direct energy source.

lowest LCOH (91 € /MWh), while hydrogen-derived carriers range from 180 € /MWh for ammonia (shipping transport) to 213 € /MWh for methane (pipeline transport), representing the upper end of the LCOH range. This outcome is expected because hydrogen-derived pathways require additional synthesis and reconversion stages, such as ammonia synthesis, methanation, or methanolization, followed by cracking or reforming at the import terminal. These extra units increase capital costs and introduce conversion losses, leading to higher energy consumption per unit of delivered hydrogen.

These results are consistent with the LCOH reported by Hampp et al. [9], ranging from 3 € /$kg_{H_2}$ (≈ 100 € /$MWh_{H_2}$) for hydrogen transported via pipelines, to 3.4 € /$kg_{H_2}$ (≈ 113 € /$MWh_{H_2}$) for hydrogen via shipping. For hydrogen-derived carriers, they report 6 € /$kg_{H_2}$ (≈200 € /$MWh_{H_2}$) for ammonia via shipping, 6.2 € /$kg_{H_2}$ (≈206 € /$MWh_{H_2}$) for methanol via shipping, and 7 € /$kg_{H_2}$ (≈233 € /$MWh_{H_2}$) for methane via pipelines.

Despite the significant gap in LCOH between hydrogen and hydrogen-derived carriers, these carriers may still be considered attractive because existing infrastructure and possible integration with other industrial systems (such as ammonia and methane networks) can reduce overall costs [10], even though this is not captured in our model. Moreover, decades of operational experience with ammonia and methane handling may make them more appealing despite their higher costs, especially when considering the safety risks associated with hydrogen [10].

On the transport side, shipping is generally more cost-effective than pipelines, except for hydrogen, where pipeline delivery avoids liquefaction losses and thus achieves a lower LCOH. Among the hydrogen-derived options, ammonia remains the most competitive due to mature synthesis and cracking processes, followed by methanol, and finally methane.

When the conversion back to hydrogen is excluded, the levelized cost of energy (LCOE, €/$\text{MWh}_{\text{LHV, carrier}}$) shows a smaller cost gap between hydrogen and the other chemicals. In this case, ammonia reaches costs comparable to hydrogen. Although methane has a higher LCOH than methanol, its LCOE is actually lower. This outcome could change if existing fossil gas infrastructure were taken into account, as this study adopts a greenfield approach in which no prior infrastructure is considered. Under such conditions, methane could become more competitive.

In this study, pathways are compared using the LCOH to provide a common functional output across all carriers. Nevertheless, the carrier LCOE remains equally relevant for decision-making. Hydrogen and its derivatives may be used directly, reconverted, or applied as chemical feedstocks, and the future distribution of these uses remains uncertain. LCOH and LCOE should therefore be regarded as complementary metrics rather than alternatives. We focus on LCOH to ensure comparability of the modeled supply chains, particularly in line with the Belgian federal focus on importing hydrogen [37], while acknowledging that LCOE is necessary to evaluate carrier-specific uses.

Moving on to the optimal configuration of each pathway, we observe that, consistent with the cost results, hydrogen carrier pathways are the least investment-demanding across all technologies (Figure 4).

Among the hydrogen-derived carriers, ammonia requires the lowest PV and wind capacities: 20.7 GW of total PV and wind, followed by methane with 23.0 GW of total PV and wind, and then methanol, which requires the largest generation capacities at 26.3 GW of total PV and wind with shipping as transportation option. Regarding the electrolyzer, methane surpasses methanol in the shipping pathway, with 11.9 GW compared to 11.5 GW, while in the pipeline pathway both ammonia (13.4 GW) and methane (14.8 GW) exceed methanol (11.5 GW). For hydrogen storage, methane and ammonia exhibit similar capacities of 20.0 GWh and 17.7 GWh in the shipping pathway, respectively, whereas methanol requires significantly higher storage at 58.9 GWh. A similar pattern is observed for batteries: hydrogen, ammonia, and methane pathways have near-zero battery capacities (below 1 GWh), while methanol reaches 14.7 GWh. This high electricity production and storage requirement for methanol is due to the fact that the methanol synthesis unit needs to operate continuously at a minimum flow.

The differences between hydrogen and hydrogen-derived pathways are largely explained by the conversion losses at the destination, which for hydrogen-derived carriers significantly outweigh the additional energy

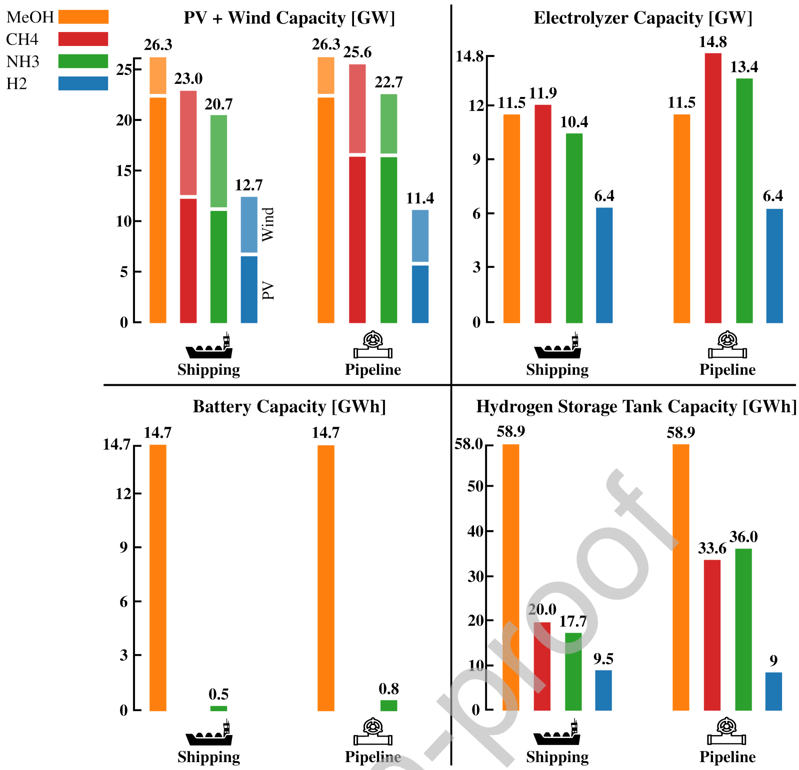


Figure 4: Installed capacities for the optimized pathways, showing that the hydrogen pathway requires the lowest overall capacities, while methanol has the largest energy storage and electricity generation capacities. Methane exhibits the highest electrolyzer capacity. The high storage and generation requirements for methanol come from the minimum power/hydrogen intake flow constraint of the methanolization unit.

required for hydrogen liquefaction in the liquid hydrogen (shipping) pathway. This is reflected in the energy consumption of the different hydrogen production and transportation pathways (defined as the ratio of total generated renewable electricity to the delivered hydrogen energy) shown in Table 1. For hydrogen, the energy consumption ranges from 1.64 $MWh_{elec}/MWh_{H_2}$ to 1.81 $MWh_{elec}/MWh_{H_2}$, whereas for the other carriers it ranges from 2.75 $MWh_{elec}/MWh_{H_2}$ to 3.52 $MWh_{elec}/MWh_{H_2}$.

| | **Hydrogen** | **Ammonia** | **Methane** | **Methanol** |
|---|---|---|---|---|
| **Shipping** | 1.81 | 2.97 | 3.33 | 2.76 |
| **Pipeline** | 1.64 | 2.98 | 3.52 | 2.75 |

Table 1: Energy consumption for each pathway [$MWh_{elec}/MWh_{LHV,H_2}$]

The cost breakdown shows that the main cost driver is different for the different hydrogen production and transportation pathways (Figure 5). For hydrogen, ammonia, and methane, wind installations account for the largest share of total costs, while for methanol, PV installations dominate, showing the critical role of solar generation in methanol production. The electrolyzer typically ranks third, except in the ammonia pipeline pathway, where it becomes the main contributor, followed by wind and PV. The second-largest contributors are carrier-specific technologies: hydrogen liquefaction for hydrogen shipping, direct air capture for carbon-based carriers, and ammonia synthesis for ammonia. Other major contributors include ammonia cracking for ammonia, steam reforming and heat pumps for methane, and methanol synthesis for methanol. These conversion-related technologies substantially raise the LCOH, exceeding the additional costs of hydrogen-specific processes such as liquefaction and liquid hydrogen storage. Furthermore, even shared technologies like wind and electrolysis cost more in hydrogen-derived pathways than in the hydrogen pathway, consistent with the higher capacities installed in these pathways.

### *3.2. Near-optimal solution space*

Following the application of MGA to the energy system optimization model for each hydrogen production and transportation pathway, the resulting near-optimal solution spaces reveal great diversity in technology capacities, as illustrated by the estimated probability density functions shown in Figure 6. The estimated probability densities provide a reliable representation of the underlying near-optimal solution spaces thanks to the large number of solutions sampled from the convex hull using the MAA method. A comparison between the sampled data histograms and the estimated probability density functions is provided in the Supplementary Information. Wind capacity, for instance, ranges from zero up to about 10 GW for the hydrogen and methanol pathways, and reaches as high as 20 GW for methane and ammonia. PV capacity shows an even broader range, extending from zero to roughly 20 GW for hydrogen, up to 35 GW for ammonia, and around 40 GW for methane and methanol. However, for methanol, PV capacity does not reach zero, but instead starts at around 12 GW. Electrolyzer capacity also exhibits great flexibility: while it cannot reach zero, as hydrogen production is essential, it varies between roughly 5 GW and 25 GW depending on the carrier. Regarding storage capacities, battery storage, which is absent in the cost-optimal configurations for hydrogen, ammonia, and methane, emerges in near-optimal designs with capacities reaching up to 60 GWh. Hydrogen storage, on the other hand, ranges from zero to 50 GWh for hydrogen, 100 GWh for ammonia and methane, and, for methanol, never reaches zero, varying instead between 16 GWh and 162 GWh.

What stands out here is that both generation and storage technologies can, in theory, be entirely excluded for hydrogen, ammonia, and methane systems, while electrolyzer capacity can be reduced to roughly 60% of its optimal value. Hence, for these three carriers, there are no 'must-have' technologies apart from the electrolyzer. Methanol systems, however, deviate from this pattern, requiring non-zero minimum capacities for both PV and hydrogen storage. It is important to note that system design cannot be approached as simple 'cherry picking'. In fact, when one technology is constrained or excluded, trade-offs arise that reshape the capacities required for others. This will be further discussed in Subsection 3.3.

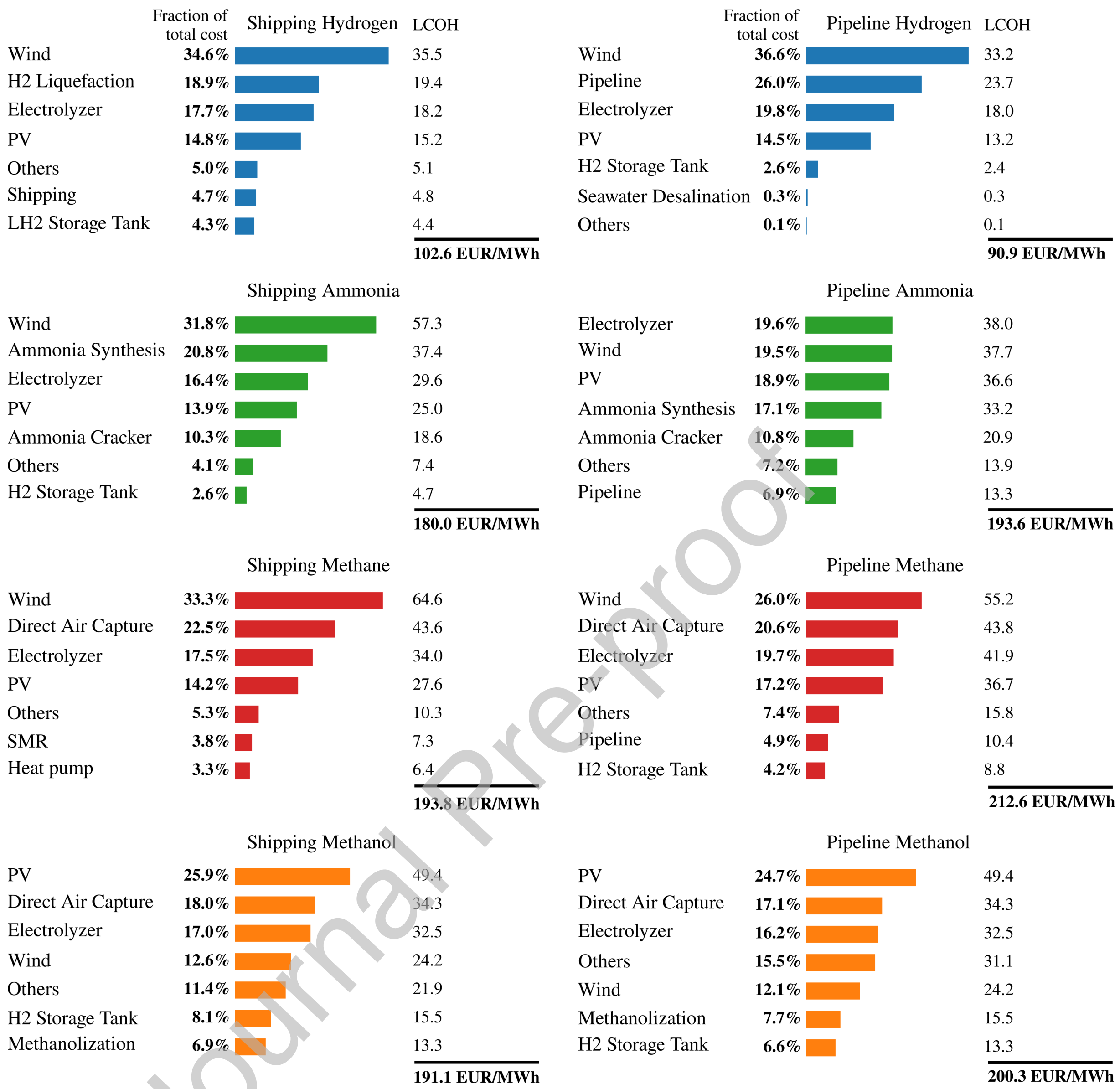


Figure 5: The cost breakdown of the optimized pathways shows that wind constitutes the largest share of total annualized system costs (left column) for the hydrogen, ammonia, and methane pathways, whereas PV is the primary cost driver for methanol. Hydrogen-derived carriers face higher overall costs due to the additional conversion units (e.g., ammonia synthesis and direct air capture), which are added to the costs of shared infrastructure such as renewable generation and electrolysis.

Finally, the cost-optimal configuration (indicated by the dot in Figure 6) does not coincide with the mode of the near-optimal distributions. This indicates that the optimal design is not the most typical configuration within the design space. In other words, while the cost-optimal point minimizes the objective function, it represents a relatively less common combination of technology capacities. By contrast, the

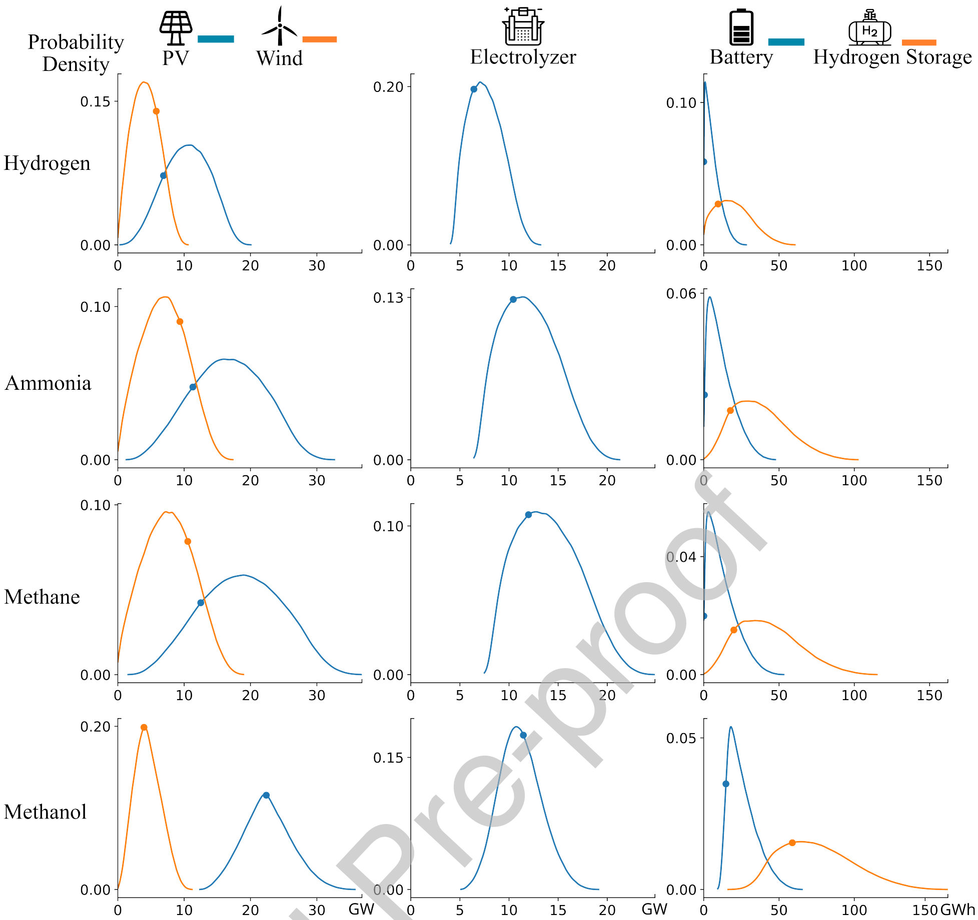


Figure 6: Probability density plots of the near-optimal solution space for the shipping pathways. The distributions illustrate the wide range of feasible capacities that remain within 10% of the minimum LCOH. The dot indicates the cost-optimal configuration. Across carriers, the near-optimal designs exhibit great diversity: PV, wind, and electrolyzer capacities vary widely, while battery storage appears in near-optimal configurations despite being absent in the optimal ones. Overall, there are no 'must-have' technologies, as most technologies (except the electrolyzer) can be entirely excluded for most carriers.

mode (or its neighboring region) corresponds to configurations that appear more frequently across the near-optimal solutions. Thus, focusing solely on the mathematical optimum risks overlooking the diversity of equally competitive designs that may better align with alternative technical, institutional, or stakeholder preferences.

An extended analysis of the near-optimal solution spaces is provided in the Supplementary Information, where two-dimensional projections of the near-optimal regions are overlaid for the four shipping pathways to compare between carriers.

### 3.3. Turning the near-optimal solution space into actionable decisions

As shown in Subsection 3.2, the near-optimal space includes a wide variety of technology combinations, where multiple system configurations achieve similar costs and many technologies are not strictly required. While this diversity highlights the flexibility of hydrogen production and transportation pathways, it also complicates interpretation, as the relationships between technologies are highly interdependent. To extract actionable insights from this large set of solutions, we apply clustering and decision trees (as detailed in Subsection 2.4) to identify the most influential decisions and clarify how constraining or excluding certain technologies affects the remaining system design. The analysis presented here focuses on the shipping pathways, as they capture the main design trade-offs across carriers. Similar patterns were found for the pipeline pathways, but are omitted for brevity.

We first apply the $k$-prototypes clustering and decision tree methods to the hydrogen-derived carriers dataset to identify the main decisions across import pathways (Subsection 3.3.1). We then perform a carrier-specific analysis using $k$-means clustering and decision trees to explore pathway-specific trade-offs in greater detail (Subsection 3.3.2).

#### 3.3.1. Decisions across hydrogen-derived import pathways

Figure 7 illustrates how system design decisions influence the choice among hydrogen-derived carriers: ammonia, methane, and methanol. At this stage, the analysis is restricted to hydrogen-derived carriers because hydrogen systems differ significantly in both cost and capacity. Only shipping pathways are shown here and the corresponding decision tree for pipeline pathways, which follows similar trends, is provided in the Supplementary Information. Each node in the decision tree splits the solution space according to a key decision variable (i.e., the features): PV, wind, electrolyzer, battery, or hydrogen storage capacity. These splits represent structural design choices and their system-wide implications, such as increased PV deployment, which is shown in the distribution of the remaining feasible configurations in Figure 7. The branches are then analyzed to identify distinct design patterns.

The first and most influential decision concerns wind capacity (feature importance = 0.60). At the far-right branch, where wind capacity is high, the need for large PV and storage capacities decreases, while electrolyzer capacity is slightly reduced. Under these conditions, only ammonia and methane remain viable import pathways, whereas methanol is no longer represented within the near-optimal solution space (57.3% of the remaining viable designs correspond to methane pathways, 42.3% to ammonia pathways, and only 0.5% to methanol pathways). This result reflects the characteristics of the near-optimal space rather than the broader feasible design space. High wind capacities provide a relatively stable renewable supply, reducing the need for additional storage and PV generation. In contrast, methanol synthesis in the TRACE model is subject to a minimum-load constraint of 90% of nominal capacity [9], requiring a stable supply of electricity and hydrogen. Thus, methanol pathways are strongly coupled with storage and PV deployment. While

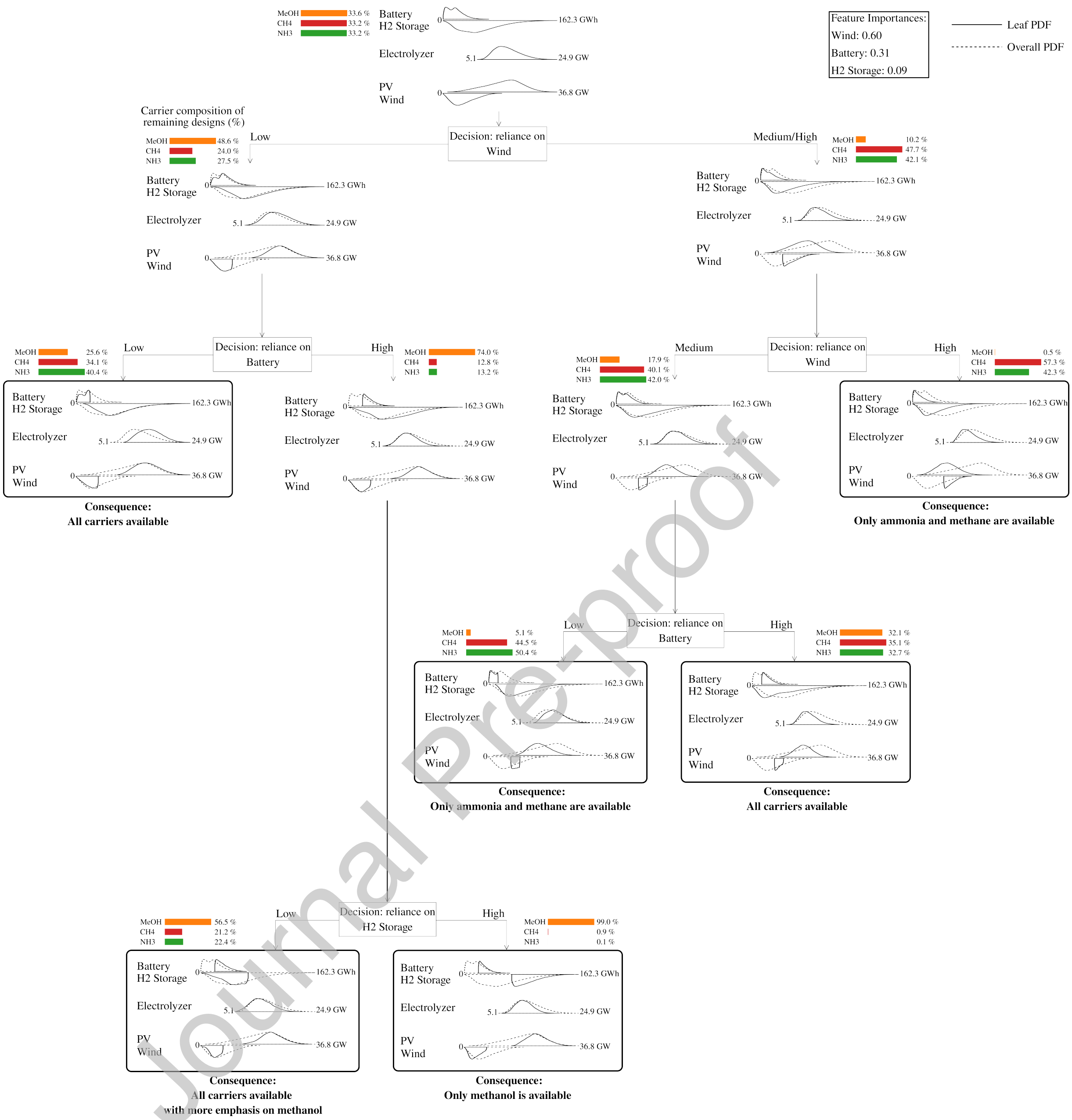


Figure 7: Carrier classification decision tree showing how renewable generation and storage capacities influence the selection of hydrogen-derived carrier import pathways within the near-optimal space. The extracted feature importances indicate that decisions related to wind capacity have the greatest influence on carrier selection, followed by battery and hydrogen storage capacities. High wind capacities lead to low PV and storage levels and therefore primarily favor ammonia and methane pathways, as shown by the fraction of remaining near-optimal designs associated with each carrier after applying the decision rule at a given node. Whereas low wind capacities, lead to high PV deployment and promote methanol, particularly when combined with large battery and hydrogen storage. At medium wind capacities, battery capacity becomes the key decision variable: low battery capacities again favor ammonia and methane, while high battery capacities allow all three carriers to remain feasible. The tree thus reveals three design archetypes: wind-dominated systems using ammonia or methane, mixed wind–PV configurations accommodating all carriers, and low-wind systems relying on methanol.

wind-dominated methanol configurations remain feasible, they do not appear within the 10% near-optimal space. Therefore, projects emphasizing large wind farms, whether driven by resource availability, policy, or stakeholder preferences, are largely limited to ammonia- or methane-based imports within the near-optimal space.

At medium wind capacities, the next decisive variable is battery storage (feature importance = 0.31). When battery capacity is low, the system again converges toward ammonia and methane pathways, as limited storage does not provide the operational flexibility required for methanol synthesis (5.1% of the remaining viable designs correspond to methanol pathways, 44.5% to methane pathways, and 50.4% to ammonia pathways). When battery capacity is high, however, all three carriers remain feasible (32.1% of the remaining viable designs correspond to methanol pathways, 35.1% to methane pathways, and 32.7% to ammonia pathways). The additional flexibility provided by batteries mitigates renewable variability, smoothing the power supply to electrolyzers and synthesis units and thereby reopening the possibility of methanol as a carrier.

Moving to the left branch of the tree, low wind capacity leads to higher PV deployment together with slightly larger electrolyzer and hydrogen storage capacities. Under these conditions, methanol re-emerges as the most frequent carrier (48.6% of the remaining viable designs correspond to methanol pathways, 24.0% to methane pathways, and 27.5% to ammonia pathways). The increased reliance on PV generation creates a greater need for storage, which aligns well with the requirements of the methanol pathway.

Within this branch, the next key decision variable is battery capacity. Choosing low battery capacity increases electrolyzer and hydrogen storage capacities, a combination that can support all three carriers (25.6% of the remaining viable designs correspond to methanol pathways, 34.1% to methane pathways, and 40.4% to ammonia pathways). In contrast, high battery capacity reduces the required electrolyzer capacity and leads mainly to methanol pathways; ammonia and methane together account for only about a quarter of the feasible import configurations (74.0% of the remaining viable designs correspond to methanol pathways, while ammonia and methane pathways together account for the remaining 26.0%).

Finally, in the low-wind, high-battery branch, hydrogen storage forms the last decision layer (with feature importance 0.09). High hydrogen storage capacity, combined with high battery capacity, low wind, and high PV power, results in smaller electrolyzers operating at steady output and eliminates ammonia and methane entirely, leaving methanol as the sole remaining option (99.0% of the remaining viable designs correspond to methanol pathways).

Taken together, Figure 7 reveals three main design archetypes. Wind-dominated designs favor ammonia or methane as the energy carrier and operate with low PV and storage capacities. Mixed wind–PV systems accommodate all three carriers and offer the greatest design flexibility, with methanol pathways limited to configurations with high storage. Finally, low-wind systems with large PV and storage capacities are mainly methanol-based. The tree also highlights the strong coupling between ammonia and methane, which share similar branches and design conditions. Methanol, in contrast, exhibits a distinct design archetype characterized by low wind capacity and high PV and storage requirements.

#### *3.3.2. Carrier-specific decisions*

Following the interpretation of the near-optimal space for all hydrogen-derived carriers combined, in this section, we will dive deeper into the decisions related to a specific carrier pathway. We start by discussing the hydrogen pathway, followed by the methanol import pathway. The decision trees for ammonia and methane, which are similar to that of hydrogen, are provided in the Supplementary Information.

For the hydrogen case, the decision tree shows that the most influential decisions concern wind power capacity, followed by battery capacity (Figure 8). These two variables drive most of the variation in system design and determine how other technologies are sized to remain within the near-optimal cost range.

The first key decision concerns wind capacity (feature importance = 0.80). Choosing low wind capacity requires decision-makers to deploy higher PV generation, larger electrolyzer capacity, and greater hydrogen storage (leftmost branch). In these cases, PV capacity lies toward the upper end of its range (8.8 GW to 20 GW). The electrolyzer and hydrogen storage capacities follow similar upward trends, with most near-optimal designs clustering at higher values. The flexibility regarding battery capacity, however, remains largely unchanged.

When wind capacity is high (rightmost branch), the pattern reverses. These configurations require less PV installation, smaller electrolyzers, and reduced hydrogen storage. Both PV and electrolyzer capacities fall within the lower half of their respective ranges, while hydrogen storage also decreases, as indicated by the skewness of its density distribution.

Between these two extremes, the model identifies a middle case where wind and PV capacities are more balanced. In these configurations, battery capacity plays a secondary role (feature importance = 0.20): low battery capacity has little impact, whereas higher battery capacity reduces the need for electrolyzer and hydrogen storage.

Although configurations that exclude either wind or PV power entirely are technically feasible, they are rare within the near-optimal set and limit flexibility for other technologies. In contrast, systems with low or no storage capacities are more common, demonstrating that storage can be constrained without significantly deviating from the near-optimal range. Overall, no technology is strictly required, but each decision influences the others. In practice, reducing one technology, such as wind, PV, or storage, necessitates compensating increases elsewhere, underscoring the strong interdependence among all components.

For the methanol case (Figure 9), the decision patterns differ from those of the other carriers. As discussed in Subsection 3.2, PV capacity is never excluded, and storage capacities, both battery and hydrogen, are generally higher. Although the feasible range of storage capacities extends to low values, the associated

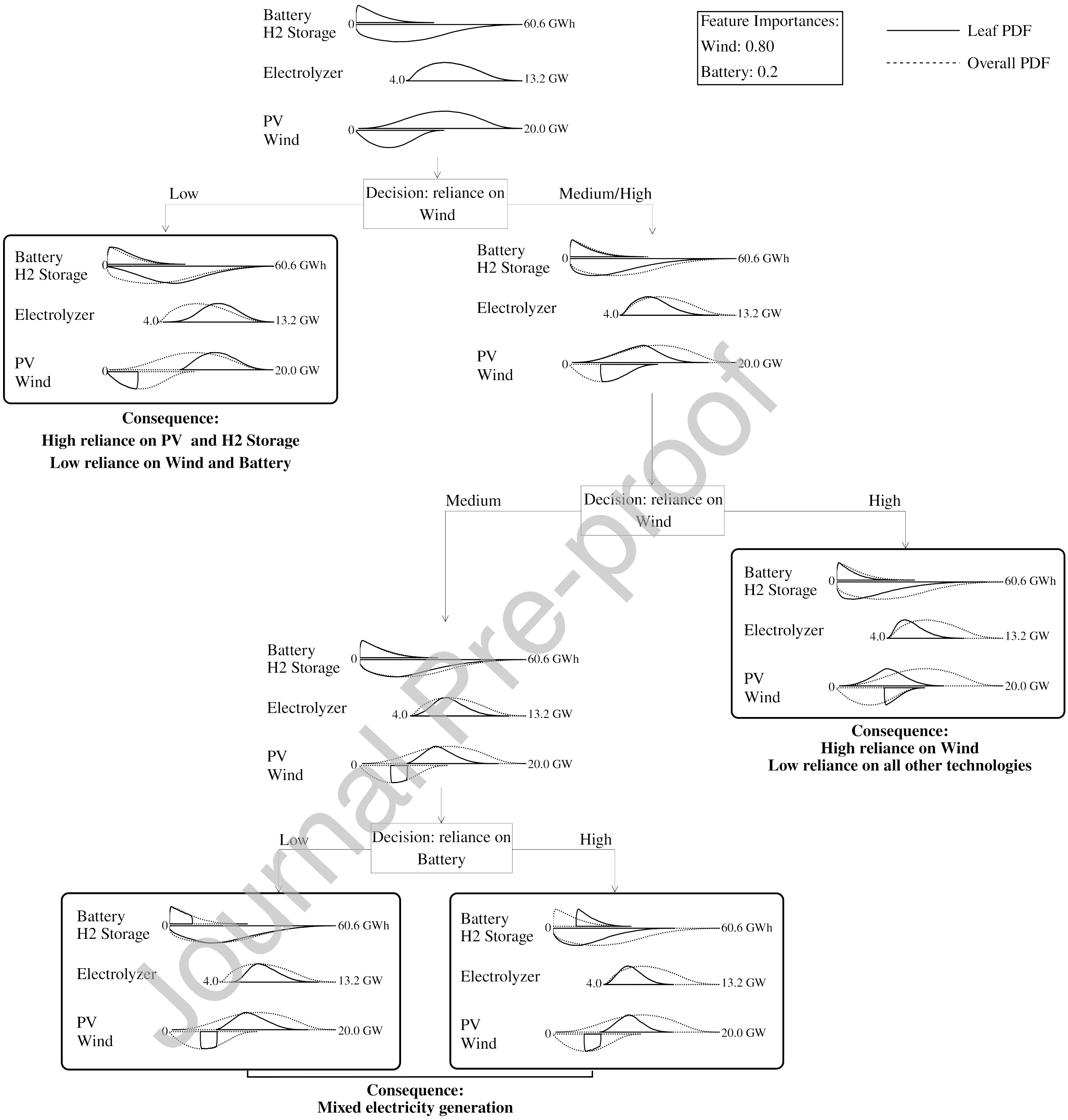


Figure 8: Decision tree for the hydrogen pathway showing how key design decisions affect the rest of the system. The first decision concerns wind capacity (feature importance = 0.80): low wind capacity leads to higher PV generation, larger electrolyzer capacity, and greater hydrogen storage, whereas high wind capacity reduces the need for these technologies. In between, a balanced mix of PV and wind allows smaller electrolyzer and storage capacities when battery capacity is high.

density is very small, indicating that most near-optimal methanol systems rely on high storage levels.

The first node splits the solutions according to wind power capacity (feature importance = 0.77). Unlike the other carriers, this decision has only a minor influence on the rest of the system. Moving from the left branch (low wind) to the right branch (high wind) does not significantly reduce the need for PV, storage, or electrolyzer capacities. The density plots remain nearly identical across branches, with only a slight decrease in PV and electrolyzer capacities at higher wind levels.

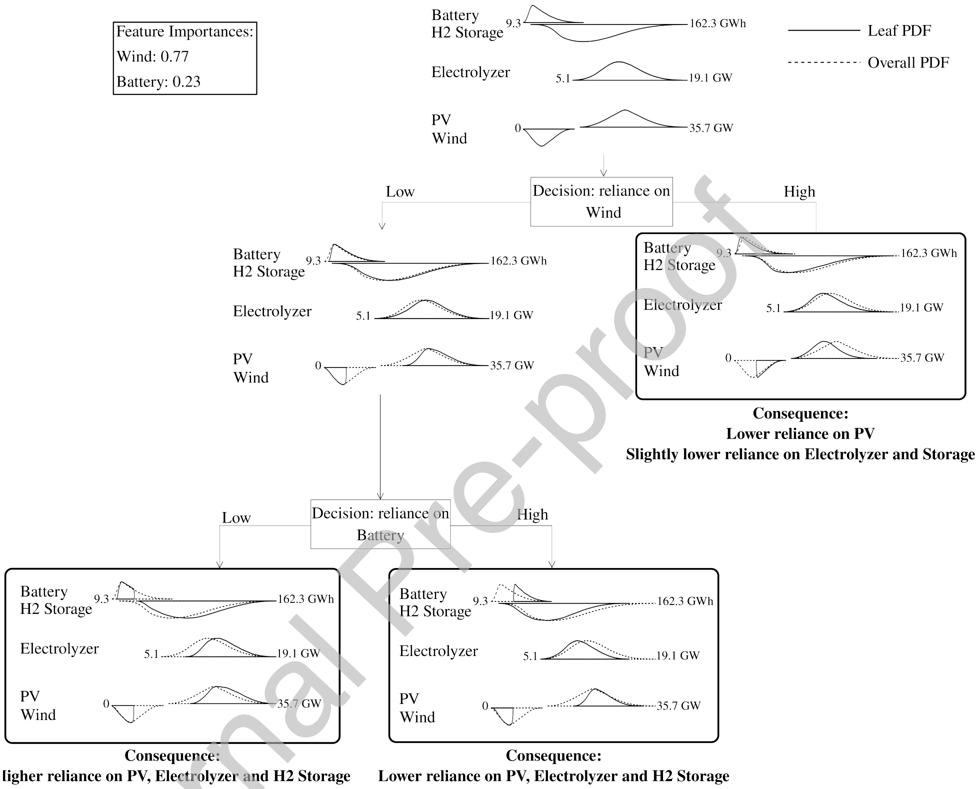


Figure 9: Decision tree for the methanol pathway showing how key design choices shape the near-optimal system configurations. The first node separates designs by wind power capacity (feature importance = 0.77), which, unlike for other carriers, has little effect on PV, electrolyzer, or storage capacities. The second node splits by battery capacity (feature importance = 0.23), where higher battery capacity slightly reduces PV, electrolyzer, and hydrogen storage requirements.

The second node concerns battery capacity (feature importance = 0.23). Along the upper branch, where battery capacity is high, the system moves toward an archetype with slightly lower electrolyzer, hydrogen storage, and PV capacities. Along the lower branch, where battery capacity is low, these capacities slightly increase. However, the changes remain small compared to those observed for the other carriers, indicating limited interdependence among design variables.

Overall, the methanol pathway shows weaker trade-offs in comparison to the others. Nearly all near-optimal designs feature relatively high PV generation and hydrogen storage capacities, regardless of wind or battery choices. This suggests that methanol systems depend on stable, solar-driven electricity and substantial storage to sustain continuous operation, while variations in wind and battery capacity play only a secondary role.

## 4. Discussion

Stakeholders rarely pursue purely techno-economic optimality: instead, they balance costs with risk, institutional feasibility, and other practical considerations [26]. Hence, it is essential to move beyond single cost-optimal solutions and explore near-optimal alternatives that remain economically comparable but differ in their technical and institutional characteristics. Equally important is to organize these alternatives in an interpretable way to ensure transparent communication of insights. In this regard, applying interpretable machine learning methods to MGA results reveals decision patterns within the near-optimal space, clarifying the trade-offs involved in energy investment decisions and showing how designs can adapt when circumstances change.

For hydrogen imports from Morocco to Belgium, the analysis of hydrogen-derived carriers shows that wind-dominated pathways, which favor hydrogen production and transport chains based on ammonia or methane, align with a preference for proven technologies and relatively predictable operations. These designs are easier to coordinate and can fit within existing industrial and regulatory frameworks [43]. Ammonia benefits from a mature global shipping network and established safety standards [44], while synthetic methane can leverage existing gas infrastructure and operational experience [45]. Because they build on familiar assets and require fewer novel technologies, such pathways are generally easier to finance and approve, reducing implementation risk. For wind-rich coastal regions such as Morocco, these systems are therefore attractive from both technical and regulatory perspectives.

In contrast, PV-dominated configurations align most closely with methanol pathways. The liquid nature of methanol simplifies storage and transport and may improve public acceptance compared with hydrogen or methane [46]. In addition, the established industrial experience in methanol handling [9] supports its deployment. In areas with limited access to strong wind resources, or where stakeholders prioritize PV deployment, such as the Noor project [21], methanol pathways can provide a viable alternative, provided that sufficient storage investments are made.

Between these two poles, mixed wind–PV configurations occupy a valuable middle ground within the near-optimal landscape. They remain economically competitive while preserving all carrier options, offering flexibility as policies, regulations, and financing conditions evolve [47].

This interpretation applies only within the hydrogen-derived carrier framework. When hydrogen itself is included as a transport carrier, the comparison changes fundamentally because its cost advantage relative to the other carriers must also be considered.

Beyond carrier selection, the analysis shows that substantial flexibility remains even after choosing a specific carrier. For instance, while the general trend in Subsection 3.3.1 suggests that ammonia and methane based systems are favored under high wind capacity, the carrier-specific decision trees in Subsection 3.3.2 reveal that low-wind configurations can still be feasible and cost-competitive. This flexibility becomes especially relevant once projects move into construction. If market conditions or supply-chain shocks render one direction impractical, decision-makers have other alternative configurations already identified within the same cost range. For example, if disruptions in the supply of rare earth metals delay wind turbine deployment [48], Subsection 3.3.2 shows that systems can compensate by relying more heavily on PV and storage. In contrast, if safety concerns or environmental impacts limit the large-scale deployment of lithium-based batteries [49, 50], designs may shift toward wind-oriented configurations, reducing the dependence on storage.

These findings hold under three main assumptions. The first concerns the production site, which in our case is Morocco. Morocco is a renewable-rich region with high wind and solar potential; therefore, the results can also be applied to other regions with similar characteristics, such as other North African countries [51]. Second, model assumptions may affect the results, for instance in the case of methanol, where a constant production flow is required in the TRACE model [9].

Despite these dependencies, the framework itself is transferable to other regions and model scopes by adapting input data and renewable resource profiles. The main takeaway is that near-optimal exploration reveals multiple cost-comparable yet structurally distinct ways to produce and transport hydrogen. No single technology mix is essential. Wind, PV, and mixed systems each occupy their own portion of the near-optimal space, offering viable options that depend on context, infrastructure, and policy priorities. This diversity shows that hydrogen supply chains can take many equally viable forms within similar cost bounds. Importantly, uncovering this range is only possible through near-optimal exploration using MGA, which is therefore essential for identifying the full spectrum of practical and policy-relevant alternatives for hydrogen imports from renewable-rich locations to high-demand areas.

The study nevertheless has several limitations that should guide future research. First, the model used here is linear, which neglects the dynamic behavior of individual components (e.g., electrolyzer load dynamics) and, importantly in the context of MGA, economies of scale. Given the large flexibility in installed capacities, ranging from none to maximum capacity, assuming a constant unit cost across the entire range is not fully realistic. A more accurate representation would involve higher unit costs at the lower end of the capacity range. Second, all parameters in this study are deterministic. While this approach highlights the design implications of decisions, it does not capture the influence of input variability, such as changes in technology costs, efficiencies, or renewable availability, on the outcomes [15, 52]. Future work will extend the framework with parametric uncertainty analysis to assess the robustness of near-optimal configurations under uncertain techno-economic and operational conditions. Third, this work is limited to a single production site in Morocco. While this allows for a detailed exploration of a specific export–import corridor, it does not capture the potential trade-offs associated with alternative production locations characterized by different renewable resource profiles. Extending the analysis to multiple exporting regions would reveal a broader range of near-optimal import strategies capable of meeting the same hydrogen demand through different combinations of production locations, energy carriers, and supply chain configurations. Finally, the definition of near-optimality depends on the allowed cost slack in MGA. The 10% slack used here is common [28], yet subjective: reducing it would narrow the design space and suppress diversity. Moreover, the MGA approach applied in this work limits the number of decision variables, leaving out other design parameters that may also be of interest.

## 5. Conclusion

In this work, we explored the near-optimal space of hydrogen import pathways, considering diversity in technology capacities and carriers, and streamlined it into key actionable decisions. This approach overcomes the limitation of relying solely on the single mathematically optimized solution, which is vulnerable to non-quantifiable constraints that can restrict the decision space, making it infeasible or undesirable.

The near-optimal space revealed a vast design range, in which technologies (except the electrolyzer) can be entirely excluded while maintaining a cost increase below 10% of the optimal LCOH. Given the large number of near-optimal solutions, extracting clear information for decision-makers is challenging. Therefore, a combination of clustering and decision trees was employed to streamline these outputs into actionable insights.

In the case of a hydrogen corridor between Morocco and Belgium, the results show that ammonia and methane share similar design characteristics, relying more on wind and less on other technologies, whereas methanol systems depend more on PV and storage and less on wind. For a given carrier, three main design archetypes were identified: a PV-dominated archetype with high electrolyzer and hydrogen storage usage and low wind deployment; a wind-dominated archetype with limited use of other technologies, resulting in storage-free designs; and a mixed electricity generation archetype, where battery capacity influences electrolyzer sizing, with higher battery capacity leading to lower electrolyzer capacity.

More generally, the proposed framework, combining MGA and interpretable machine learning, can be applied to other regions and models and can support decision-makers in understanding available design options and their consequences. These insights not only present alternative configurations but also help derive clear decision-making rules and identify trade-offs, such as the need for higher wind capacities when large storage capacities are not desired or feasible. This can assist in aligning design choices with site characteristics and facilitate clearer communication of project attributes to stakeholders from the early stages of planning.

Future work will focus on applying this method to broader applications, such as transition models with pathway formulations, as well as improving the MGA method to include parametric uncertainty and to overcome dimensional limitations.

### Supplementary information

Supplementary information is available for this paper.

### CRediT authorship contribution statement

**Mahdi Kchaou:** Conceptualization, Data Curation, Formal Analysis, Investigation, Methodology, Software, Validation, Visualization, Writing – Original Draft, Writing – Review & Editing. **Francesco Contino:** Conceptualization, Visualization, Writing – Review & Editing. **Diederik Coppitters:** Conceptualization, Formal Analysis, Methodology, Supervision, Validation, Visualization, Writing – Original Draft, Writing – Review & Editing.

### Declaration of competing interest

All authors have no competing interests.

### Acknowledgments

This work was supported by the Wallonie-Bruxelles International - WBI (M.K); and the Fonds de la Recherche Scientifique - FNRS [CR 40016260] (D.C).



### References

[1] The European Commission, REPowerEU Plan, The European Commission, Brussels, 2022.

[2] K. V. Vilbergsson, K. Dillman, N. Emami, E. J. Ásbjörnsson, J. Heinonen, D. C. Finger, Can remote green hydrogen production play a key role in decarbonizing europe in the future? a cradle-to-gate lca of hydrogen production in austria, belgium, and iceland, International Journal of Hydrogen Energy 48 (46) (2023) 17711–17728. doi:doi.org/10.1016/j.ijhydene.2023.01.081.

[3] K. Verleysen, D. Coppitters, A. Parente, F. Contino, Where to build the ideal solar-powered ammonia plant? design optimization of a belgian and moroccan power-to-ammonia plant for covering the belgian demand under uncertainties, Applications in Energy and Combustion Science 14 (2023) 100141. doi:doi.org/10.1016/j.jaecs.2023.100141.

[4] T. H. Roos, The cost of production and storage of renewable hydrogen in south africa and transport to japan and eu up to 2050 under different scenarios, International Journal of Hydrogen Energy 46 (72) (2021) 35814–35830, special Issue on HYPOTHESIS XV. doi:doi.org/10.1016/j.ijhydene.2021.08.193.

[5] H. Ishaq, I. Dincer, C. Crawford, A review on hydrogen production and utilization: Challenges and opportunities, International Journal of Hydrogen Energy 47 (62) (2022) 26238–26264, sI: Progress in Hydrogen Production, Storage and Distribution (Ahmadi). doi:doi.org/10.1016/j.ijhydene.2021.11.149.

[6] G. Brändle, M. Schönfisch, S. Schulte, Estimating long-term global supply costs for low-carbon hydrogen, Applied Energy 302 (2021) 117481. doi:doi.org/10.1016/j.apenergy.2021.117481.

[7] Hydrogen Import Coalition, Shipping sun and wind to belgium is key in climate neutral economy, Flux50 (2021).

[8] V. Dias, M. Pochet, F. Contino, H. Jeanmart, Energy and economic costs of chemical storage, Frontiers in Mechanical Engineering Volume 6 - 2020 (2020). doi:10.3389/fmech.2020.00021.

[9] J. Hampp, M. Düren, T. Brown, Import options for chemical energy carriers from renewable sources to germany, PLOS ONE 18 (2) (2023) 1–31. doi:10.1371/journal.pone.0281380.

[10] J. Cui, M. Aziz, Techno-economic analysis of hydrogen transportation infrastructure using ammonia and methanol, International Journal of Hydrogen Energy 48 (42) (2023) 15737–15747. doi:10.1016/j.ijhydene.2023.01.096.

[11] C. Johnston, M. H. Ali Khan, R. Amal, R. Daiyan, I. MacGill, Shipping the sunshine: An open-source model for costing renewable hydrogen transport from Australia, International Journal of Hydrogen Energy 47 (47) (2022) 20362–20377. doi:10.1016/j.ijhydene.2022.04.156.

[12] T. Galimova, M. Fasihi, D. Bogdanov, C. Breyer, Impact of international transportation chains on cost of green e-hydrogen: Global cost of hydrogen and consequences for germany and finland, Applied Energy 347 (2023) 121369. doi:10.1016/j.apenergy.2023.121369.

[13] T. Galimova, M. Fasihi, D. Bogdanov, C. Breyer, Feasibility of green ammonia trading via pipelines and shipping: Cases of europe, north africa, and south america, Journal of Cleaner Production 427 (2023) 139212. doi:10.1016/j.jclepro.2023.139212.

[14] D. Coppitters, A. Costa, R. Chauvy, L. Dubois, W. De Paepe, D. Thomas, G. De Weireld, F. Contino, Energy, exergy, economic and environmental (4e) analysis of integrated direct air capture and co2 methanation under uncertainty, Fuel 344 (2023) 127969. doi:doi.org/10.1016/j.fuel.2023.127969.

[15] G. Mavromatidis, K. Orehounig, J. Carmeliet, A review of uncertainty characterisation approaches for the optimal design of distributed energy systems, Renewable and Sustainable Energy Reviews 88 (2018) 258–277. doi:doi.org/10.1016/j.rser.2018.02.021.

[16] D. Coppitters, W. De Paepe, F. Contino, Surrogate-assisted robust design optimization and global sensitivity analysis of a directly coupled photovoltaic-electrolyzer system under techno-economic uncertainty, Applied Energy 248 (2019) 310–320. doi:10.1016/j.apenergy.2019.04.101.

[17] N. Wolf, M. A. Tanneberger, M. Höck, Levelized cost of hydrogen production in northern africa and europe in 2050: A monte carlo simulation for germany, norway, spain, algeria, morocco, and egypt, International Journal of Hydrogen Energy 69 (2024) 184–194. doi:doi.org/10.1016/j.ijhydene.2024.04.319.

[18] N. Korem, O. Duek, R. Jia, E. Wertheimer, S. Metviner, M. Grubb, I. Levy, Modeling decision-making under uncertainty with qualitative outcomes, PLOS Computational Biology 21 (3) (2025) 1–18. doi:10.1371/journal.pcbi.1012440.

[19] M. Lewis, The us's largest solar farm is canceled because nevada locals don't want to look at it, Available online: https://electrek.co/2021/07/26/us-largest-solar-farm-is-scrapped-because-nevada-locals-dont-want-to-look-at-it/. Accessed: 19th March 2025 (2021).

[20] T. A. Faunce, J. Prest, D. Su, S. J. Hearne, F. Iacopi, On grid batteries for large scale energy storage: Challenges and opportunities for policy and technology, MRS Energy & Sustainability 5 (2018) 10. doi:10.1557/mre.2018.11.

[21] A. Eljechtimi, Moroccan solar plans hampered by dispute over technology, Available online: https://www.reuters.com/world/africa/moroccan-solar-plans-hampered-by-dispute-over-technology-2024-02-27/. Accessed: 6th March 2025, reuters (2024).

[22] P. Lombardi, How a storm of lawsuits paralysed wind mills in northwest spain, Available online: https://www.reuters.com/business/energy/how-storm-lawsuits-paralysed-wind-mills-northwest-spain-2025-01-14/. Accessed: 19th March 2025 (2025).

[23] F. Pflugmann, N. de Blasio, The geopolitics of renewable hydrogen in low-carbon energy markets, Geopolitics, History, and International Relations 12 (2020) 9–44.

[24] L. Flath, C. Quittkat, Mapping the hydrogen power players: An analysis of lobbying on eu hydrogen policy-making, International Journal of Hydrogen Energy 130 (2025) 538–547. doi:10.1016/j.ijhydene.2025.04.214.

[25] A. G. Palanca, et al., Bridging the gap: Public perception and acceptance of green hydrogen technology in the philippines, Sustainability 17 (1) (2025) 324. doi:10.3390/su17010324.

[26] E. D. Brill, The use of optimization models in public-sector planning, Management Science 25 (5) (1979) 413–422. doi:10.1287/mnsc.25.5.413.

[27] S.-Y. Chang, E. D. Brill Jr., L. D. Hopkins, Use of mathematical models to generate alternative solutions to water resources planning problems, Water Resources Research 18 (1) (1982) 58–64. doi:10.1029/WR018i001p00058.

[28] J. F. DeCarolis, Using modeling to generate alternatives (MGA) to expand our thinking on energy futures, Energy Economics 33 (2) (2011) 145–152. doi:10.1016/j.eneco.2010.05.002.

[29] F. Neumann, T. Brown, The near-optimal feasible space of a renewable power system model, Electric Power Systems Research 190 (2021) 106690. doi:10.1016/j.epsr.2020.106690.

[30] F. Lombardi, B. Pickering, E. Colombo, S. Pfenninger, Policy decision support for renewables deployment through spatially explicit practically optimal alternatives, Joule 4 (10) (2020) 2185–2207. doi:10.1016/j.joule.2020.08.002.

[31] T. T. Pedersen, M. Victoria, M. G. Rasmussen, G. B. Andresen, Modeling all alternative solutions for highly renewable energy systems, Energy 234 (2021) 121294. doi:10.1016/j.energy.2021.121294.

[32] A. Sinha, A. Venkatesh, K. Jordan, J. Johnson, Diverse decarbonization pathways under near cost-optimal futures, Nature Communications 15 (8165) (2024) 52433. doi:10.1038/s41467-024-52433-z.

[33] M. G. Prina, R. M. Johannsen, W. Sparber, P. A. Østergaard, Evaluating near-optimal scenarios with energyplan to support policy makers, Smart Energy 10 (2023) 100100. doi:doi.org/10.1016/j.segy.2023.100100.

[34] F. J. Baader, S. Moret, W. Wiesemann, I. Staffell, A. Bardow, Streamlining energy transition scenarios to key policy decisions (2023). arXiv:2311.06625.

[35] T. Brown, J. Hörsch, D. Schlachtberger, PyPSA: Python for Power System Analysis, Journal of Open Research Software 6 (4) (2018). doi:10.5334/jors.188.

[36] Oxford Analytica Daily Brief, Morocco will be a major player in green hydrogen, Available online: dailybrief.oxan.com/Analysis/DB275094/Morocco-will-be-a-major-player-in-green-hydrogen. Accessed: 5th September 2024 (2023).

[37] FPS Economy, Vision and strategy - Hydrogen, Available online: https://economie.fgov.be/en/themes/energy/sources-and-carriers-energy/hydrogen/belgian-federal-hydrogen. Accessed: 28th February 2025 (2022).

[38] C. B. Barber, D. P. Dobkin, H. Huhdanpaa, Qhull: Quickhull algorithm for computing the convex hull, Astrophysics Source Code Library, record ascl:1304.016 (Apr. 2013).

[39] Z. Huang, Extensions to the k-means algorithm for clustering large data sets with categorical values, Data Mining and Knowledge Discovery 2 (3) (1998) 283–304. doi:10.1023/A:1009769707641.

[40] Z. Huang, Clustering large data sets with mixed numeric and categorical values, 1997. URL https://api.semanticscholar.org/CorpusID:3007488

[41] P. J. Rousseeuw, Silhouettes: A graphical aid to the interpretation and validation of cluster analysis, Journal of Computational and Applied Mathematics 20 (1987) 53–65. doi:doi.org/10.1016/0377-0427(87)90125-7.

[42] L. Breiman, J. Friedman, R. A. Olshen, C. J. Stone, Classification and Regression Trees, 1st Edition, Chapman and Hall/CRC, 1984. doi:10.1201/9781315139470.

[43] C. Cao, B. Wen, Y. Fang, Z. Hou, Q. Wang, T. Zhang, L. Huang, Q. Chen, L. Zhang, Y. Zhao, et al., A comprehensive comparison of green ammonia and green methanol from a full chain: production, transportation, storage and utilization, Carbon Neutral Systems 1 (1) (2025) 8. doi:10.1007/s44438-025-00009-9.

[44] H. H. Cho, V. Strezov, T. J. Evans, Life cycle assessment of renewable hydrogen transport by ammonia, International Journal of Hydrogen Energy 94 (20) (2024) 1018–1035. doi:10.1016/j.ijhydene.2024.11.076.

[45] F. Carels, L. Sens, M. Kaltschmitt, Synthetic natural gas as a green hydrogen carrier – technical, economic and environmental assessment of several supply chain concepts, Energy Conversion and Management 321 (2024) 118940. doi:10.1016/j.enconman.2024.118940.

[46] V. J. Reddy, N. Hariram, R. Maity, M. F. Ghazali, S. Kumarasamy, Sustainable e-fuels: Green hydrogen, methanol and ammonia for carbon-neutral transportation, World Electric Vehicle Journal 14 (12) (2023) 349. doi:10.3390/wevj14120349.

[47] A. Odenweller, F. Ueckerdt, G. F. Nemet, M. Jensterle, G. Luderer, Probabilistic feasibility space of scaling up green hydrogen supply, Nature Energy 7 (9) (2022) 854–865. doi:10.1038/s41560-022-01097-4.

[48] L. Depraiter, S. Goutte, T. Porcher, Geopolitical risk and the global supply of rare earth permanent magnets: Insights from china's export trends, Energy Economics 146 (2025) 108496. doi:10.1016/j.eneco.2025.108496.

[49] Y. Chen, Y. Kang, Y. Zhao, L. Wang, J. Liu, Y. Li, Z. Liang, X. He, X. Li, N. Tavajohi, B. Li, A review of lithium-ion battery safety concerns: The issues, strategies, and testing standards, Journal of Energy Chemistry 59 (2021) 83–99. doi:10.1016/j.jechem.2020.10.017.

[50] T. Lavisse, R. Panariello, F. Perdu, S. Rolère, P. Zwolinski, Developing a methodological framework for assessing absolute sustainability in battery upscaling within planetary boundaries, Procedia CIRP 122 (2024) 766–771, 31st CIRP Conference on Life Cycle Engineering. doi:10.1016/j.procir.2024.01.106.

[51] K. Chiteka, C. Enweremadu, Harnessing africa's renewable potential with an integrated framework for energy justice and climate resilience, Discover Sustainability 6 (1) 1220. doi:10.1007/s43621-025-02119-3.

[52] F. Neumann, T. Brown, Broad ranges of investment configurations for renewable power systems, robust to cost uncertainty and near-optimality, iScience 26 (5) (2023) 106702. doi:10.1016/j.isci.2023.106702.